Lloyd's mirror for MTF testing of MISR CCD

E. B. Hochberg, N. L. Chrien

Jet Propulsion laboratory
4800 Oak Grove Drive, Pasadena, CA911 09

ABSTRACT

Direct measurement of CCD MTF using a unique Lloyd's mirror fringe projector is described. MTF measurements on the MISR linear CCD arrays have been performed as a function of spatial frequency, wavelength, number of charge transfers, radiation dosage, and device architecture. Test results arc reported here.

Keywords: MTF, CCD imaging performance, Lloyds mirror interferometer

1. INTRODUCTION

JPL's Multi-Angle imaging Spectro-Radiometer (MISR) instrument orbiting on the EOS AM 1 platform contains nine cameras employing linear CCD imaging arrays in the focal plane. The cameras use the linear arrays in pushbroom mock to form images of the earth's surface in four narrow wavelength bands between 443 nm and 865 nm. Each camera contains four 1 x 1504 pixel "strings" with a narrow band spectral filter in front of each string.

in order to verify analytic models of MISR CCD imaging performance, and thereby camera system models, a device for measuring the modulation transfer function (MTF) of MISR CCDs has been constructed. Of particular interest are measurements of MTF dependencies on device type., illumination wavelength, number of transfers, illumination level, and X-ray radiation dosage. Additionally, we are interested in MTF response before and after (proton, electron) radiation testing to determine if the CCDs would meet the end-of-life MTF performance requirement.

This paper will discuss design & performance of the variable spatial frequency fringe projector based on a Lloyd's mirror interferometer. Data reduction algorithms developed by N. Chrien and actual MISR CCD MTF test results follow.

2. THEORY

In the classical Lloyd's mirror interferometer, high visibility $\cos^2$ fringes of constant spatial frequency are formed when a monochromatic, plane (collimated) wavefront is spatially divided in half by a plane mirror and the halves are superimposed as schematically shown below.

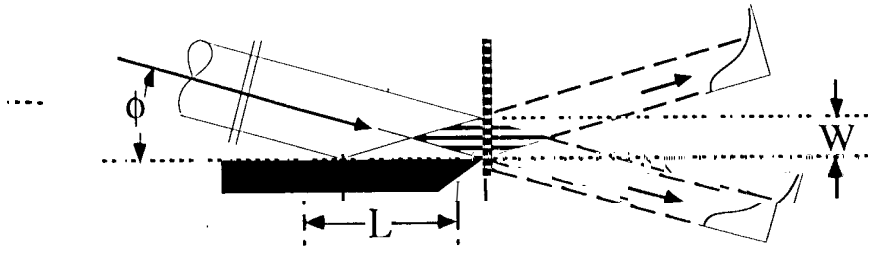

Figure 1. Lloyd's mirror interferometer.

With collimated monochromatic light, fringe spatial frequency υ is constant and dependent only upon wavelength and the angle at which the two wavefronts interfere according to:

$$\upsilon = 2\,\lambda^{-1} \sin\phi$$

where ϕ is the half-angle between the two wavefronts and λ is the wavelength

3. PRACTICE

Note MISR camera MTF performance is specified at the detector Nyquist frequency only. Thus the spatial frequencies of interest arc dictated by pixel size and pitch: MISR CCD pixel pitch is 21μm implying a Nyquist frequency υ_{Nyq} = one-half cutoff frequency = 0.5 cycle/21 μm = 23.8 cycles/mm.

Using a HeNe laser (λ = 0.6328 pm), fringes at the MISR CCD Nyquist arc formed on the CCD when the half-angle between the direct and reflected beams is 7.53 mrad or 0.432 degrees -- that is, near-normal incidence on the CCD, and near-grazing incidence on the mirror. I ,ower spatial frequency fringes are formed as the half-angle decreases, requiring longer mirrors.

In our device the collimated fringe-forming wavefront is approximated by means of a pinhole at a large distance from the interference zone pcr the schematic shown in the figure below:

Given: D, λ, E, R set: ϕ_O

Calculate: H, Z, υ, C(W), α, θ j, β, M, A, B, OPD(W), I, CCD signal

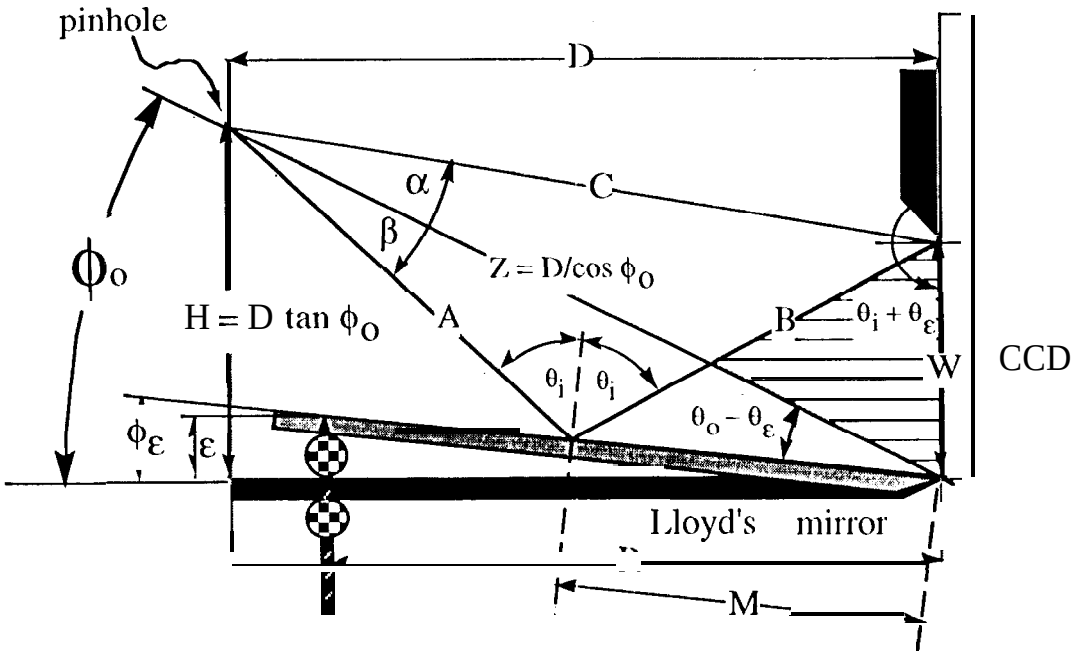

Figure 2.1 .loyd's mirror for MTF testing of CCD: geometry

Regarding the approximation to interference between truly crsllimated/piano wave.fronts: Spherical wavefronts of radius = 0.391 m i.e., that spherical wavefront emerging from a pinhole at D = 0.391 m from the CCD-end of the mirror -- can be shown to produce a negligible variation in fringe spatial frequency ("chirp") over the aperture: $\partial\upsilon/\upsilon$ = 3E-6. I'bus, sufficiently well-collimated ("flat" or piano) wavefronts arc realized without the aid of a collimator.

I;irst-order parameters of a small-angle Lloyd's mirror interferometer arc calculated including,...

- mirror length M required to project fringes over an aperture (i.e., (hc CCD) of width W
- Gaussian beam intensity 1 at aperture point W: I(W)
- CCD signal output prediction (not including charge transfer or diffusion effects)
- spatial frequency υ(W, Z) in the interference region

This last is particularly important as it allows us to treat more simply-formed spherical wavefronts of radius Z (e.g., from a pinhole) rather than collimated wavefronts ($Z = \infty$).

4. EXPERIMENT

The Lloyd's mirror fringe projector has been configured as a s[and-alone unit compatible with the vutically-oriented MISR CCD test station. Fringe frequency is adjusted by means of a single micrometer which causes mirror tilt about the knife edge of the mirror. The breadboard unit also includes an adjustable stop to mask both the direct, un-interfered portion of the wavefront from reaching the CCD and to limit the size of the interference patch on the CCD. Finally, in order to measure CTE effects over the length of the. array, the whole assembly translates up and down in order to illuminate different subapertures of the (fixed) CCD array.

Projected fringe spatial frequency υ is related to micrometer location R and excursion ε according to the following calibration relation:

$$\upsilon = 2\,\varepsilon\,\lambda^{-1}\,R^{-1} + \upsilon_0$$

For example with R = 0.318 m, the calibration factor is 9.955ε c/mm for 632.8 rrm light and 8.024ε c/mm for 785 rrm light where ε is the micrometer excursion in mm. In 632.8 nm light, an excursion of 2.39 mm scans spatial frequencies from DC to 23.8 cycles/mm; 2.97 mm excursion is required for 78S nm illumination.

S. DATA REDUCTION

The output of the CCD array in response to the Lloyd's mirr or illumination is digitized to 12 bits for each band or line array and each pixel. For each spatial frequency for which a measurement is made, a series of 10 data sets is recorded. A corresponding series of dark frame measurements arc also part of the data file: a dark frame is the CCD response with the input illumination blocked.

l'hc first step in the data reduction is to subtract the dark frame from the measured data. The second step is to find the average and standard deviation over the 10 repetitions and 4 bands for each pixel. The extent of the projected fringe pattern in the downtrack direction is relatively uniform over all four bands (fringe tilt<<1 degree). Averaging over bands and repetitions provides a larger sample for our curve fits.

The next step in the data reduction is to select the pixels over which the data will be fit for a determination of the MTF. The center 129 pixels (center pixel ± 64 pixels) of the illuminated portion of the CCD arc chosen for this purpose. This keeps us away from the edges of the illuminated area which arc more likely to be contaminated by diffraction effects from the edges of the stop and mirror.

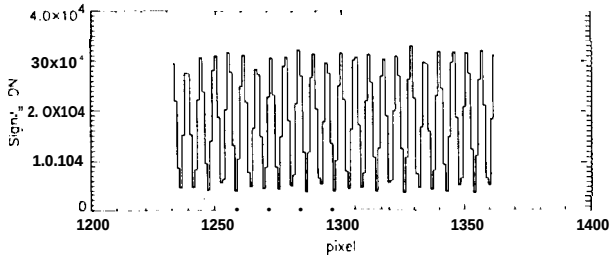

Figure 5. Sample of center 129 pixels chosen for analysis.

For each spatial frequency, a non-linear least-squares fit was made to the function:

$$S = a_0 + a_1 \cdot \cos(2 \cdot \pi \cdot 0.021 \cdot a_2 \cdot x - a_3)$$

where,

x = pixel number, S = data number output by CCD at pixel x, and 0.021 mm/pixel = pixel pitch,

From the resultant fit parameters, a_i, (he MTF of the CCD output is derived:

$$MTF_{fit} = \left|\frac{a_1}{a_0}\right|$$

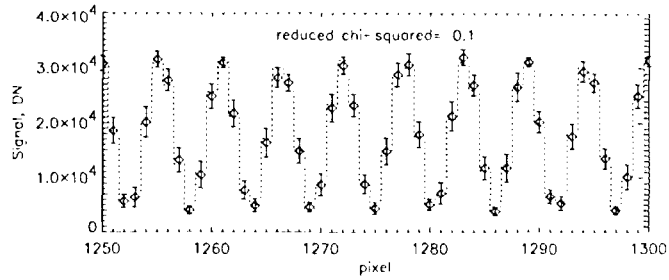

Figure 6. Expanded view of averaged data with error bars denoting ±1σ and dashed line representing best tit to data

Uncertainties of the fit parameters, σ_{a_i}, arc used to estimate the relative uncertainty in MTF_{fit}:

$$\frac{\partial(MTF_{fit})}{MTF_{fit}} = \pm\sqrt{\left(\frac{\sigma_{a_1}}{|a_1|}\right)^2 + \left(\frac{\sigma_{a_0}}{|a_0|}\right)^2} \qquad \text{(See Figure 6)}$$

The MTF of the CCD at spatial frequency v is defined as:

$$MTF_{CCD}(\nu) = MTF_{\text{CCD output}}(\nu)/MTF_{\text{projected fringes}}(\nu)$$

An informal systematic error analysis considering the effects of mirror reflectivity, flatness, polarization, setup geometry and alignment errors leads us to the conclusion that stray and scattered light effects limit the ultimate projected fringe modulation. To determine an upper bound cm the effect of stray and scattered light, we examine. the character of the MTF curve as spatial frequency approaches zero. Ideally, MTF approaches unity as the spatial frequency goes to zero. By extrapolating the measured MTF curve to its value at zero spatial frequency, wc may estimate the maximum possible degradation in the measured MTF duc to stray and scattered light effects. This varies from measurement to measurement. For example, in Figure 7a, the estimated degradation is -5% at zero c/mm spatial frequency.

6 . RADIATION TEST RESULTS

Two series of measurements were taken after the CCD devices underwent radiation testing. The first series of measurements, listed in I'able 1 in the Appendix, were designed to provide information about MTF dependencies on device type, illumination wavelength, number of transfers, illumination level, and radiation dosage. Devices I.1W19#0_O and I.1W 19#0_1 arc of thick-poly t ypc while the remaining devices arc of the thin-pol y t ypc that is to be flown on MISR.

The signal level reported is the average over all spatial frequency measurements for the data set. The equivalent reflectance is based on the assumption that a signal corresponding to 100% equivalent reflectance will produce 720,000 electrons [80% of a detector fullwell of 900,000 electrons]. The second series of measurements were taken to better map the illumination level dependence of the MTF seen after exposure to high doses of radiation. I'able 2 lists the corresponding equivalent reflectance levels. The uncertainty in equivalent reflectance shown in tbc last column of Tables 1 and 2 is calculated from the uncertainty in the signal level:

$$\partial S_{e^-} = \pm\sqrt{\left(\frac{\partial S_{DN}}{S_{DN}}\right)^2 + \left(\frac{\partial(\text{Gain})}{\text{Gain}}\right)^2} \cdot S_{e^-}$$

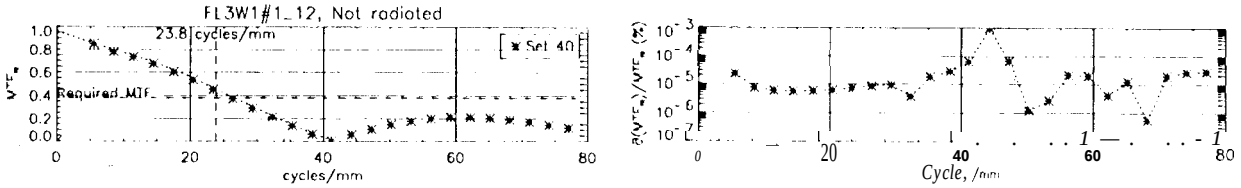

(a) (b)

Figure 7. CCD MTF of un-radiated thin-poly device.

The estimated uncertainty in the fit MTF, MTF_{fit}, shown in Figure 7b is representative of all the results in that the relative uncertainty in the calculated MTF values is typically < 0.1% (error bars arc smaller than the plot symbols). The resultant fits were generally very good (reduced $\chi^2 < 1.5$) and the uncertainties on the fit parameters were small. The main uncertainty in the measured CCD MTF, MTF_{CCD}, is in the stray light effect ($MTF_{projected\ fringes} < 1$) which, as discussed above is typically 5%.

7. WAVELENGTH DEPENDENCE

A 785 nm single longitudinal mode laser source (Spindler & Hoycr Model DC25D) was procured to assess MTF dependence at longer wavelengths where charge diffusion is hypothesized to have a larger impact on MTF.

The Lloyd's mirror setup allows fringes in either 632.8 nm (HeNe) or 785 nm ± 10nm to be projected. Experimental MTF data collected with the two lasers is shown in Figures 8 and 9:

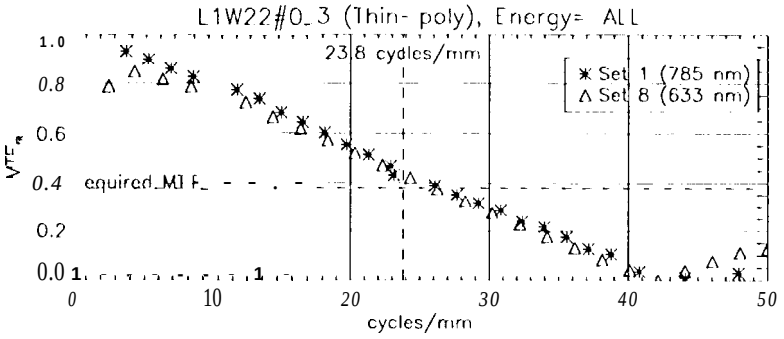

Figure 8. CCD MTF post-radiation for device L1W22#0_3 at 632.8 and 785 nm (thin-poly)

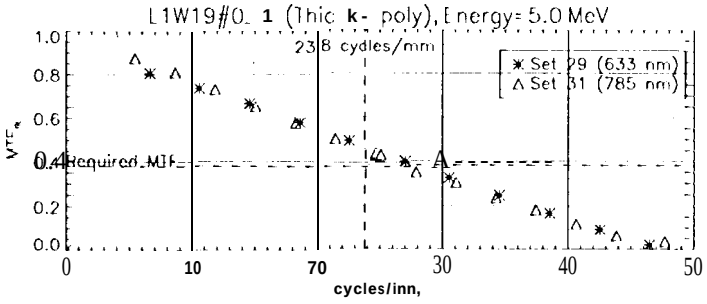

Figure 9. CCD MTF post-radiation for device L1W19#0_1 at 633 nm and 785 nm (thick-poly).

From Figures 8 and 9, we conclude that the MTF dependence on illumination wavelengths between 632.8 nm and 785 nm appears to be negligeable.

8. SIGNAL DEPENDENT MTF

The only thin-poly device which shows a significant MTF dependence on mean signal level is L1W22#0_3 which has

received all energy levels in the radiation test (Figure 12). At 23.8 c/mm, the detector Nyquist frequency, MTF falls just below the required 38% when the mean illumination level falls to 8% equivalent reflectance (Ml. Set 10). If wc assume that at 23.8 cycles/n~nl, a linear interpolation is valid between the 14% and 8% measured signal levels, then the MTF requirement of 38% is met for an equivalent reflectance of 10%.

The degradation in MTF seen in Figure 12 is indicative of a reduction in the charge transfer efficiency (CTE) of the CCD with signal level. In Figure 12a, wc sec that the degradation in MTF is also affected by the number of transfers along the array, which is again indicative of a CTE effect. This result is corroborated by post-radiation electronic CTE characterizat ion tests.

At the lowest radiation level, there is no discernible difference in MTF with signal level.

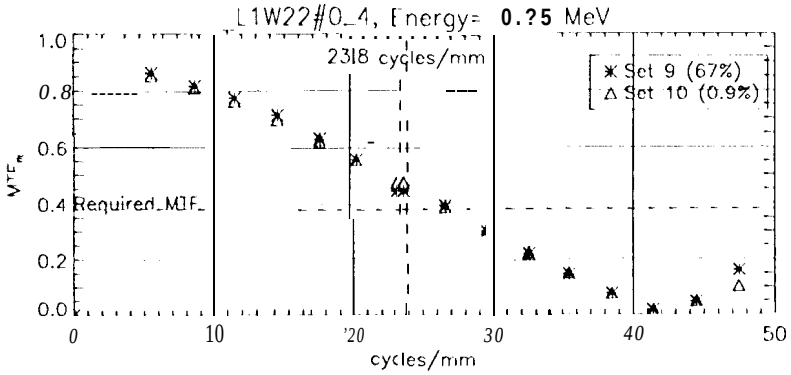

Figure 10. CCD MTF post-radiation for device L1W22#0_4 (0.25 MeV) at 632.8 nm.

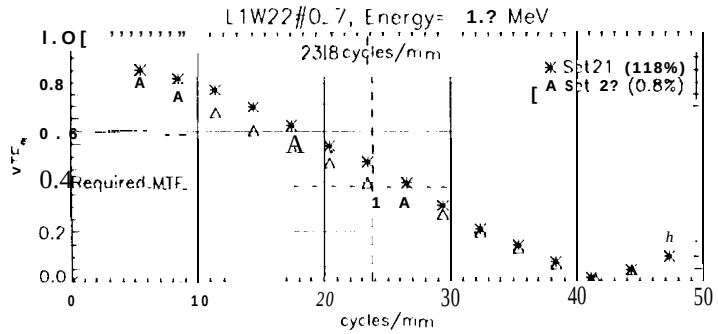

Figure 11. CCD MTF post-radiation for device L1W22#0_7 (1.2 McV) at 632.8 nm.

At the 1.2 MeV radiation energy level, only a slight dependence of MTF on signal level is seen; the required CCD MTF is still met over the range of signal levels from 1% to 10070 equivalent reflectance..

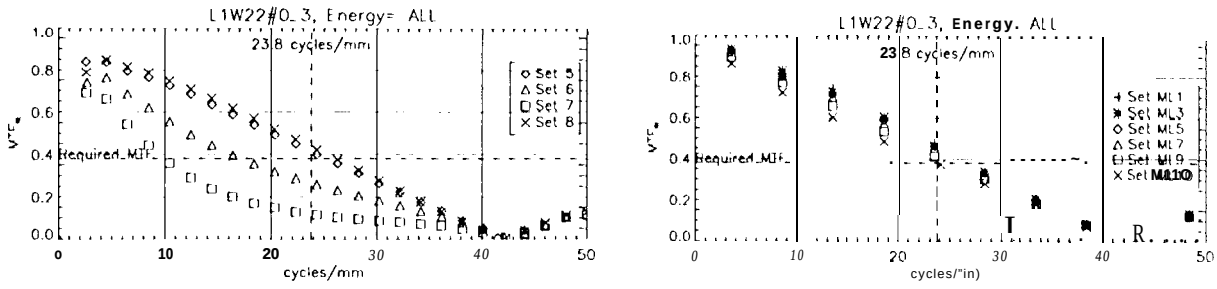

(a) (b)

Figure 12. CCD MTF post-radiation for device 1.1 W22#0_3 at 632.8 nm.

An apparent improvement in MTF of the "ML sets" of ~5% is attributed to a reduction in the stray and scattered light effects due to a small change in position of a stray light stop in the Lloyd's mirror set-up.

The thick-poly devices which were measured both show a degradation in low signal level MTF. For the thick-poly devices the only devices measured saw the 5.0 McV energy level and the aggregate of the 0.25 McV, 0.4 McV, 0.7 McV, 1.2 MeV and 5.0 MeV energy levels. The results for the two are quite similar and imply that the 5.0 McV radiation energy level is the cause of the radiation degradation witnessed in the CCD MTF.

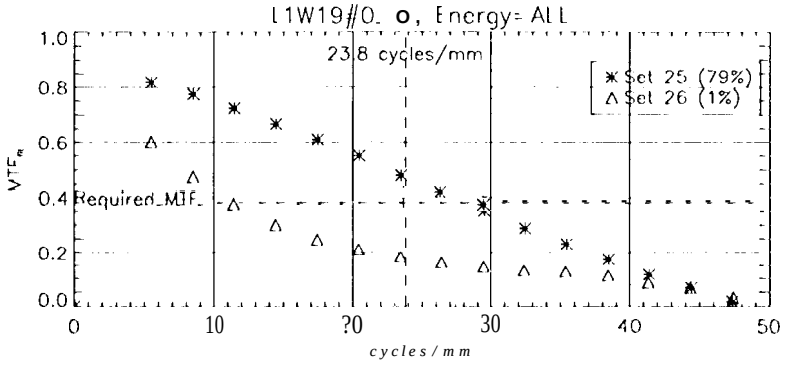

Figure 13. CCD MTF post-radiation for device L1 WI 9#0_0 at 632.8 nm with signal level,

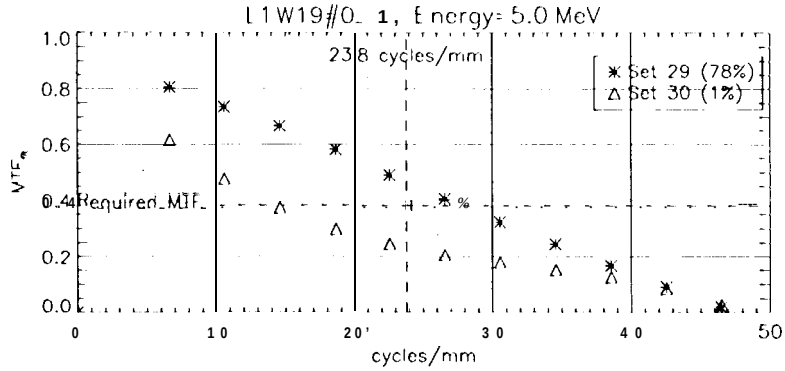

Figure 14. CCD MTF post-radiation for device L1 W19#0_1 at 632.8 nm with signal level.

9. MATHEMATICAL MODEL

Our mathematical model for predicting the CCD MTF utilizes component MTF equations for carrier diffusion and detector spatial aperture (trapezoid response function) taken from *Electro-optical hardware considerations in measuring the*

imaging capability of scanned time-delay-and-integrate charge-coupled imagers', The equation for the CTE component MTF is taken from *Optical Radiation Detectors* 2

The crosstrack CCD MTF is then mathematically modeled as:

$$MTF_{CCD,cross} = MTF_{aperture} \times MTF_{diff} \times MTF_{CTE}$$

The crosstrack CCD MTF was measured and modeled because it will suffer the most due to radiation damage induced CTE degradation and the diffusion effects will also be more pronounced in this direction. In the downtrack direction there is oniy one transfer; in the. crosstrack direction there wiii be up to 1512 transfers.

10. MEASURED RESULTS VERSUS MODEL

Significant similarities and differences between the model and our experimental measurements were observed:

Considering only the cutoff frequency, wc find good agreement between our Lloyd's mirror measurements of thick-poly t ype CCD's and the trapezoidal model: Cutoff frequency is both predicted and measured to be 47.6 c/mm. The lack of generally good agreement is attributed to the stray & scattered light problems encountered during that early phase of the testing program.

As illustrated in Figure 16, larger discrepancies are seen bet ween model and measurement for the thin poi y CCD's that wi i i be used in the fright cameras. Here, we 1) measure cutoff frequencies of -42 c/mm instead of 47.6 c/mm; 2) commensurately reduced modulation at all frequencies below the cutoff -- 42% instead of 55% at Nyquist, and 3) maximum modulation at frequencies above cutoff is higher than predicted -- 26% instead of 22%.

11. INFERRING THE PIXEL SPATIAL RESPONSE FUNCTION (PSRF)

These results led us to suspect the validity of the trapezoidal PSRF model. in principle, a Fourier transformation of our measured CCD MTF measurements will reveal the actual PSRF. However, an accurate, detailed mapping of the PSRF would require significantly more high spatial frequency MTF measurements than were actually collected during the test program. Nonetheless, carefully extrapolating the extant results beyond 80 c/mm and transforming reveals the interesting PSRF seen in Figure 17. Instead of the 21 µm fiat-topped trapezoid wc see a 21 pm-wide PSRF with peak response al the edges and lowered sensitivity in the center of the pixel.

Corroboration of this unexpected prediction is seen in camera-level testing of these devices: That is, after integration with the MISR optics, camera-level MTF testing is conducted. Camera MTF is inferred from Fourier transformation of a camera PSRF measurement which in turn results from slowly scanning an unresolved spot across a given pixel. See Figure below:

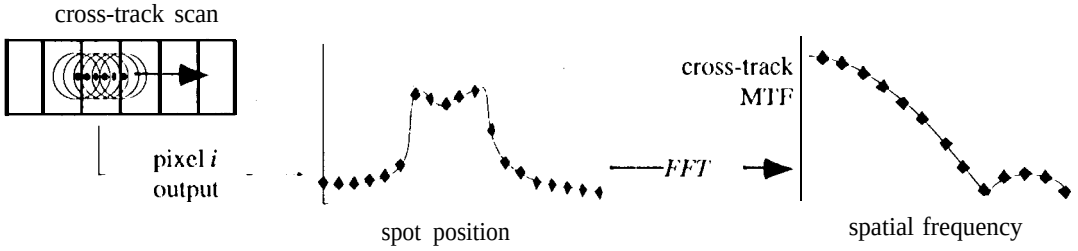

Showing measurement of camera MTF

These tests of course include MTF contributions from the optics, but these effects arc known to be relatively small compared to the CCD. Thus, during camera testing, most frequently in the red and green bands, wc again see the PSRF sensitivity dip, the 42 c/mm cutoff and the higher modulation seen at frequencies above the cutoff. That these features have not been seen in the IR band is not well understood.

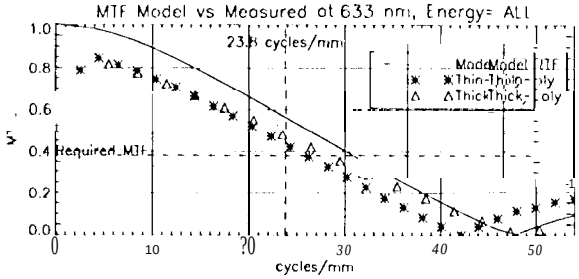

Figure 15

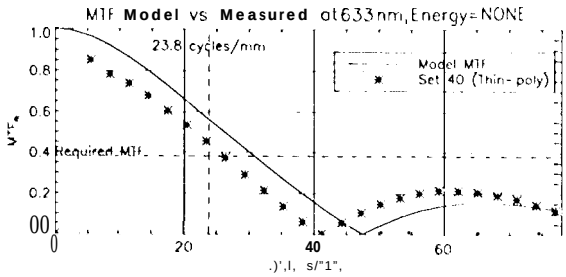

Figure 16.

Figure 15. CCD MTF at 632.8 nm, model vs. measured thin-poly (Set 8) and thick-poly (Set 25).
Figure 16. Thin-poly M-IT versus mathematical model prediction.

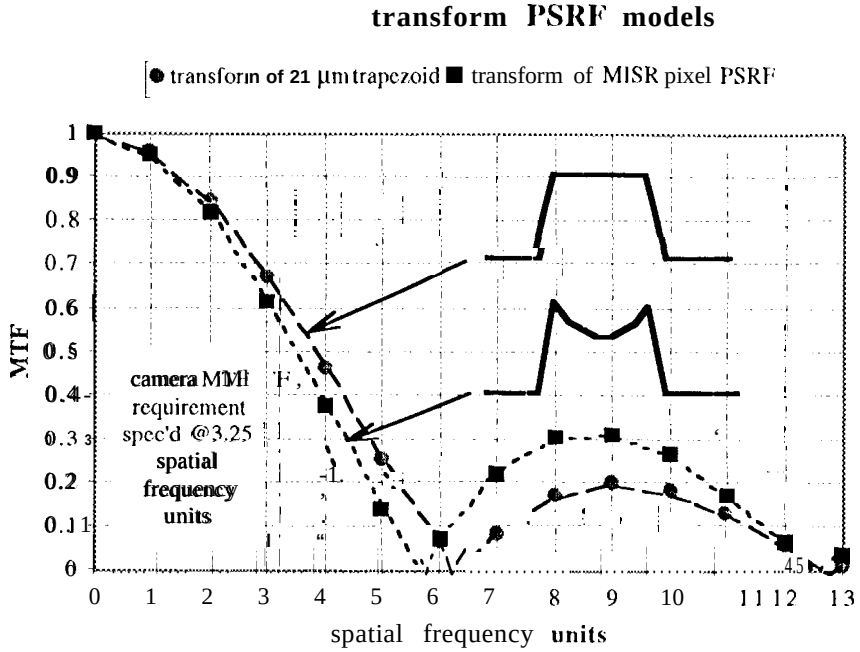

Figure 17. Example of PSRF predicted by Fourier transform,

12, CONCLUSION

The Lloyd's mirror interometer has proven to be a useful tool for quantifying CCD MTF imaging performance. Use of this device revealed that CCD MTF performance is not accurately predicted by simple. PSRF models.

13. ACKNOWLEDGMENTS

The authors would like to thank W. Conner for construction of the interferometer, Harold Johnson Jr. of Harold Johnson Optical Laboratories for donation of the. mirror, G. Nakatsukasa for aluminization of the mirror, and M. Shao for many helpful discussions.

14. APPENDIX

Table 1. Post-radiation CCD MTF measurement data sets.

Device Energy 1 evel	Set	wvl, level, transfers	Avg. Signal [DN]	Gain [e-/DN]	Signal level [e-]	Equivalent reflectance
1/1 W22#0_3	1	785 nm, FW, 1500	19,800	27.90	552,407	76.7% ± 0.9%
0.2s MeV,	2	785 nrn, 2%), 1500	1,025	1.52	1,559	0.2% ±0.0%
0.40 MeV,	3	78511111, 2%, 750	1,472	1.52	2,237	0.3% ± 0.0%
0.70 MeV,	4	785 nm, 2%, 64	1,751	1.52	2,662	0.4% ± 0.0%
1.20 MeV,	5	633 nm, 2%, 64	2,321	1.52	3,528	0.5% ± 0.0%
and 5.0 MeV	6	633 run, 2%, 750	2,475	1.52	3,76_4	0.5% ± 0.0?4
	7	633 nm, 2%, 1500	2,737	1.52	4,161	0.6% ±0.0%
	8	633 nrn, FW, 1500	20,863	27.90	582,090	80.8% ± 0.8%
1.1 W22#O_4	9	633 nm, FW, 1500	16,840	28.50	479,931	66.7% ±1.6%
0.25 MeV	10	633 nrn, 2%, 1500	4,108	1.64	6,738	0.9% ± 0.0%
	11	785 nm, FW, 1500	14,975	28.50	426,774	59.3% ± 1.9%
	12	785 nm, 2%, 1500	5,387	1.64	8,834	1.2% ±0.0%
1.1 W22#0_6	17	633 nm, FW, 1500	20,994	28.80	604,637	84.0% ±1.5%
0.7 MeV	18	633 nm, 2%, 1500	3,609	1.65	5,956	0.8% ±0.0%
	19	785 nm, FW, 1500	19,190	28.80	552,680	76.8% ± 1.5%
	20	785 nrn, 2%, 1500	4,S21	1.65	7,460	1.0% ±0.0%
1.1 W22#0_7	21	633 nrn, FW,1500	29,828	28.70	856,058	118.9% ±0.8%
1.2 MeV	22	633 nm, 2%, 1500	3,716	1.64	6,094	0.8% ±0.0%
	23	785 nm, }'W, 1500	19,597	28.70	562,447	78.1% ± 3.6%
	24	785 nm, 2%, 1500	3,589	1.64	5,886	0.8% ± 0.0%
1.l.W19#/o- o	25	633 nrn, FW, 1500	17,924	31.90	571,772	79.4% ±1.2%
0.25, 0.4,	26	633 nm, 2%, 1500	5,412	1.75	9,471	1.3% ± 0.0%
0.7, 1.2,	27	785 nrn, FW, 1500	4,657	31.90	148,550	20.6% ± 0.4%
and 5.0 MeV	28	785 nm, 2%, 1500	5,465	1.75	9,563	1.3% ± 0.0%
L1W19#0_1	29	633 mn, FW, 1500	17,613	32.00	563,605	78.3% ±1.5%
5.0 McV	30	633 nrn, 2%, 1500	6,613	1.73	11,441	1.6% ± 0.0%
	31	785 am, FW, 1500	8,522	32.00	272,691	37.9% ± 1.0 %
	32	785 run, 2%, 1500	9,420	1.73	16,296	2.3% ± 0.0%
FL3W1#1_12 Not radiated	40	633 nm, FW, 1500	17,887	29.76	532,317	73.9% ±4.0%

Table 2. CCD MTF as a function of illumination level measurement data sc(s.

Device Energy Level	Set	Avg Signal [DN]	Gain [e-/DN]	Signal level [e-]	Equivalent Reflectance
L1W22#0_3	ML1	11,733	28.39	333,035	46.3% ± 1.8%
0.25 MeV,	ML2	10,771	28.39	305,720	42.5% ± 1.2%
0.40 MeV,	ML3	9,399	28.39	266,779	37.1% ± 0.9%
0.70 MeV,	ML4	8,459	28.39	240.105	33.3% ± 0.4%
1.20 McV,	ML5	7,026	28.39	199;44 1	27.7% ± 0.8%
and 5.0 MeV	ML6	7,179	28.39	203,778	28.3% ± 0.4%
	ML7	5,859	28.39	166,304	23.1% ± 0.4%
	ML8	4,815	28.39	136,659	19.070 ±0.3%
	ML9	3,412	28.39	96,860	13.5% ± 0.2%
	ML10	2,025	28.39	57,479	8.0% ± 0.2%

CCD MTF, post-radiation, maximum transfers
Thick-poly devices:

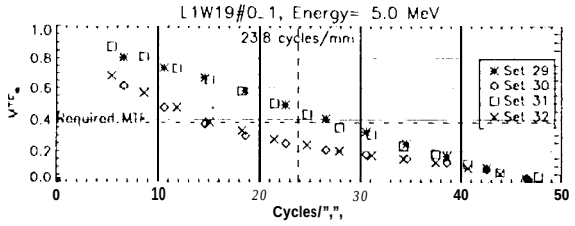

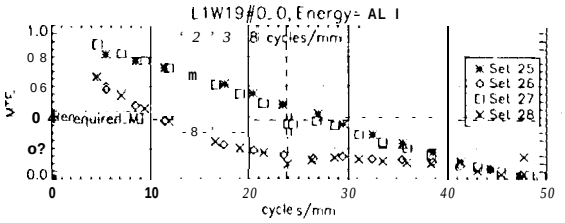

Thin-poly devices:

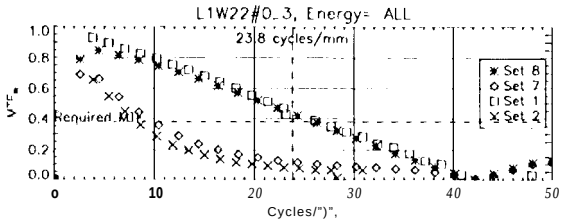

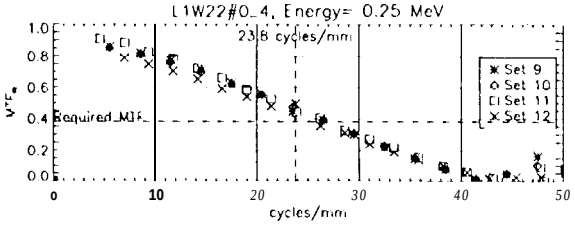

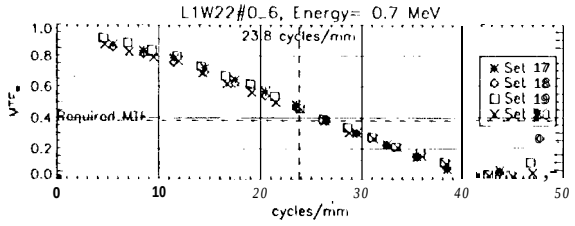

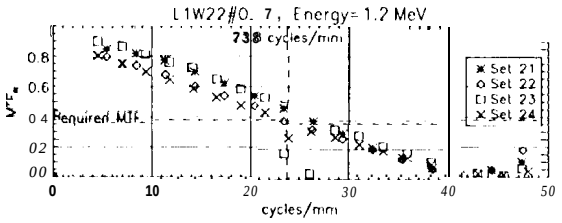

The work described in this paper was carried out by the Jet Propulsion Laboratory, California institute of Technology, under a contract with NASA.

15. REFERENCES

1. T.S. Lomheim, et al, "Electro-optical hardware considerations in measuring the imaging capability of scanned time-delay-and-intcgrale charge-coupled imagers" Optical Engineering, August, 1990

2. Dereniak & Crowe, *Optical Radiation Detectors*, John Wiley & Sons, Inc., 1984

word count 3/29/96 = 3941 incl footnotes

word count 4/1 6/96 = 4243 incl footnotes

word count 5/2/96 = 4348 incl footnotes

word count 6/20/96 = 3949 incl footnotes

word count 6/25/96 = 3272 incl footnotes